

Si-Doped Fe₂O₃ Grown by DC- RF Magnetron Co-Sputtering

Erdal Turgut^{1*} 

¹ Ataturk University, Department of Electric Power Generation, Askale Vocational College, Erzurum, Turkey

Sorumlu Yazar/Corresponding Author
E-mail:erdal.turgut@atauni.edu.tr

Araştırma Makalesi/Research Article
Geliş Tarihi/Received: 16.03.2024
Kabul Tarihi/Accepted: 05.06.2024

ABSTRACT

In this study, the structure of silicon iron oxide (Si:Fe₂O₃) was grown using co-sputtering. The Si:Fe₂O₃ film was grown on glass substrates at a pressure of 8.5 mTorr and a temperature of 450°C for 35 minutes. Optical measurements were revealed that the band gap of the structure ranged from 2.54 to 2.73 eV. The roughness values of the obtained films were observed as Ra 3.08 nm and Sa 2.7 nm for Si:Fe₂O₃, and Ra 1.88 nm and Sa 2.09 nm for Fe₂O₃, respectively. As obtained from XPS data, the change in binding energy was observed to depend on the electron exchange between silicon, iron and oxygen. In the iron-silicon oxide structure, the energy increased slightly as a result of the chemical environment. The Si⁴⁺ ion had a strong tendency to distribute itself within the tetrahedral region of spinel-like structures. The behavior of the structure was influenced by the stoichiometry of oxygen. The consistent results from both XRD and SEM images indicated that the crystal grain sizes gradually decreased as the silicon content increased.

Keywords: Silicon iron oxide, Co-sputtering, Spinel-like structures, Thin film, Semiconductor

DC-RF Magnetron Ortak Püskürtme ile Yetiştirilen Si-Katkılı Fe₂O₃

ÖZ

Bu çalışmada silikon demir oksidin (Si:Fe₂O₃) yapısı ortak saçırma kullanılarak büyütüldü. Si:Fe₂O₃ filmi, 8.5 mTorr basınçta ve 450°C sıcaklıkta cam taban malzemeler üzerinde 35 dakika süreyle büyütüldü. Optik ölçümler, yapının bant aralığının 2.54 ila 2.73 eV arasında değiştiğini ortaya çıkardı. Elde edilen filmlerin pürüzlülük değerleri Si:Fe₂O₃ için sırasıyla Ra 3.08 nm ve Sa 2.7 nm, Fe₂O₃ için ise Ra 1.88 nm ve Sa 2.09 nm olarak gözlemlendi. XPS verilerinden elde edildiği gibi, bağlanma enerjisindeki değişim silikon, demir ve oksijen arasındaki elektron alışverişine bağlı olduğu gözlenmiştir. Demir-silisyum oksit yapısında kimyasal ortamın etkisiyle enerjinin bir miktar arttığı görüldü. Si⁴⁺ iyonu, spinel benzeri yapıların tetrahedral bölgelere yerleşme konusunda güçlü bir eğilime sahip olduğu görüldü. Yapının davranışının, oksijenin stokiyometrisinden etkilendiği sonucunu ortaya koydu. Hem XRD hem de SEM görüntülerinden elde edilen tutarlı sonuçlar, silikon içeriğinin artması ile kristal tane boyutlarının giderek azaldığını gösterdi.

Anahtar Kelimeler: Silikon demir oksit, Birlikte püskürtme, Spinel benzeri yapılar, İnce Film, Yarı iletken

Cite as;

Turgut, E. (2024). Si-Doped Fe₂O₃ Grown by DC- RF Magnetron Co-Sputtering. *Recep Tayyip Erdogan University Journal of Science and Engineering*, 5(1), 133-140. Doi: 10.53501/rteufemud.1450119

1. Introduction

Soft magnetic metal oxide structures consist of magnetic particles coated with an insulating material. It is widely used in the construction of commonly used tools such as inductors, sensors, transformers, and electric motors (Shokrollahi and Janghorban, 2007; Leary et al., 2012; Xiong et al., 2013). The magnetic properties of electrical machines have a very important effect on the energy conversion process and also on the performance of the machine. With this in mind, in order to increase the energy efficiency of these machines, it is important to consider the magnetic core characteristics in the context of working conditions as well as production processes. The most commonly studied processes in the literature are cutting, welding, pressing or shrinking magnetic cores (Bali et al., 2017; Helbling et al., 2020). For example; Magnetic circuits used in industrial applications are heat treated after being processed with dielectric materials under a certain vacuum pressure (Hu et al., 2010; Uebe et al., 2012). With the increasing demands in technology, the development of magnetic materials and devices with low magnetic loss and also high saturation magnetization under high frequency, which are widely used in electricity and electronics, is a serious problem (Bourchas et al., 2016). The main cause of high-frequency magnetic loss is due to eddy current loss, and the eddy current loss occurring in soft magnetic structured materials consists of intra-particle and inter-particle eddy current loss. Optimizing the composition of magnetic materials is a very important method to reduce eddy current losses in the material. The use of additives is an effective way to compound iron oxide. Therefore, 6.5% Si doping causes the structure to exhibit relatively high electrical resistance as well as low eddy current loss. Eddy current loss between particles in the material is related to the electrical resistance of the materials, this loss can be reduced by adding high resistance materials to the structure (Wei et al., 2011; Silveyra et al., 2018). The most commonly used method to reduce eddy current is to create an insulating layer on the surface. In recent years, it has aimed to focus on the selection

and synthesis of suitable insulation materials (Chomoucka et al., 2010; Yamazaki and Fukushima, 2015; Helbling et al., 2020). Magnetite nanoparticles are frequently used in magnetic resonance imaging, production of contrast agents, magnetic separation and sorting of cells and proteins, pathology laboratories, and a variety of biomedical applications, including hyperthermia therapy for cancer tumors (Zhu et al., 2013). Considering the importance of magnetite nanoparticles In recent years, there has been an increase in the synthesis of magnetic nanoparticles (Xiao et al., 2011; Chu et al., 2013; Zhang et al., 2011)

2. Materials and Methods

Silicon iron oxide thin films (Si:Fe₂O₃) were grown using DC magnetron and RF magnetron sputtering techniques simultaneously. In general terms, the sputtering technique is the process of removing atoms or molecules from the target by sending inert gas to a metal target. It is the deposition of these atoms or molecules removed from the surface as a thin film on the base material, which is located in a cell under vacuum and has a certain base temperature.

Argon (Ar) gas is often used as an inert gas to remove atoms or molecules from the target material surface. The inert gas used is converted into plasma with the help of RF or DC power supply. The plasma hits the metal surface on the target material with high momentum and removes atoms or molecules from the surface.

In our study, the diameter of the silicone target material placed in the RF gun source was selected as 2 inches and its thickness as 0.125 inches. In addition, the diameter of the iron target placed in the DC power gun was determined as 2 inches and its thickness was determined as 0.005 inches.

In this experimental study, the DC power supply was selected as 120 watts and the RF power supply was selected as 40 watts. After the bottom pressure was reduced to 5×10^{-6} Torr, the glass substrates placed in the vacuum cell were heated to 450 degrees. After these procedures, plasma

was created by sending 100 sscm of inert argon gas under vacuum to the cell. Then, 40 sscm of argon and 3 sscm of oxygen gas were introduced into the chamber with a growth pressure of 8.5×10^{-3} Torr and the growth process was carried out for 35 minutes.

Thus, Si:Fe₂O₃ crystalline thin films were grown on glass substrate under 8.5 mTorr pressure. Crystal structures of the films were analyzed by XRD using X-ray diffractometer in the θ -2 θ Bragg Brentana configuration (CuK α ($\lambda = 1.5405 \text{ \AA}$)). In addition, Tapping Atomic Force Microscopy (AFM) images of the thin films were obtained. Si:Fe₂O₃ SEM images of thin films were taken with a Zeiss Sigma 300 SEM device. XPS measurements were carried out using the Flex Mod Specs XPS system. An Al anode was used as the X-ray source.

3. Result and Discussion

X-rays can easily penetrate the crystal structure of any material and give us information about the properties of the material when exiting that material.

This is why X-ray diffraction is very useful technique for the characterization of different types of materials. We can easily calculate the size of particles from Debye Scherrer formula given: Debye Scherrer Formula:

$$D = (0.94 \times \lambda) / (\beta \times \cos\theta) \quad (1)$$

Where, D = Average crystallite size, β = line

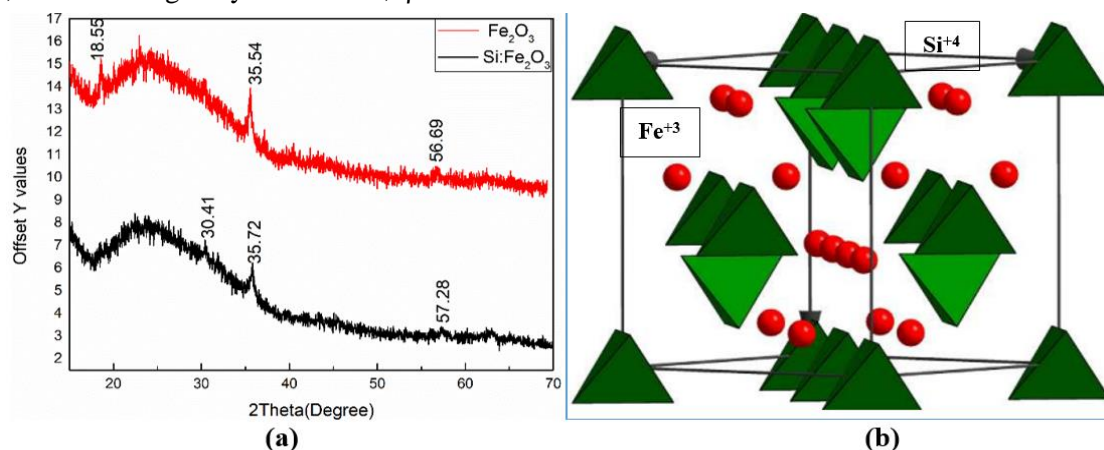


Figure 1. (a) XRD patterns of Si:Fe₂O₃ and Fe₂O₃ structure (b) The spinel structure: the octahedral B sites are represented by red balls and the AO₄ units are plotted as green tetrahedra (Piekarz et al., 2010)

broadening in radians (FWHM; Full Width at Half Maximum), θ = Bragg angle, λ = X-Ray wavelength. Average crystal sizes were calculated by the Debye Scherrer method and according to the calculation results, Fe₂O₃ crystal was calculated as 20 nm and Si:Fe₂O₃ crystal was calculated as 17 nm.

Figure 1(a) shows the XRD diffraction patterns of maghemite iron oxide (Fe₂O₃) with a tetragonal crystal structure. According to the XRD diffraction pattern, it was observed that distinct peaks occurred in the Fe₂O₃ phase at 18.55°, 35.54° and 56.69° (Qayoom et al., 2020).

The crystal structure of Si:Fe₂O₃ thin films also has a tetragonal structure, and the XRD diffraction patterns of both compounds are shown together in Figure 1(a). It has been observed that the peak value of the Si:Fe₂O₃ structure appears quite clearly at 30.41° (Lee et al., 2013).

According to the XRD results taken to examine the structural properties, it was observed that the lattice parameters, especially the grain size, gradually decreased as the silicon content increased. The Si⁴⁺ cation in spinel-like structures showed a strong distribution tendency in the tetrahedral region, which was affected by the oxygen content Figure 1(b). It was observed that the grain size decreased significantly with the amount of silicon added into the structure, and there was a relatively small change in the lattice distortion (Schoppa et al., 2003).

Raman data measured at room temperature and in the wavelength range of 0–3500 cm⁻¹ were obtained. Raman measurements were taken for pure and Si-doped magnetites (Si:Fe₂O₃), which give very reliable information about the chemical structure and crystal structure environment. Figure 2 specifically shows the Raman spectrum for the pure Fe₃O₄ structure and according to group theory A_{1g} = 679.83, T_{2g}(1) = 493.53, T_{2g}(2) = 326.62 and T_{2g}(3)=194.24 cm⁻¹. Raman's active modes have been identified. There are many sources regarding these data in other studies (Gasparov et al., 2000; Piekarcz et al., 2010). It was observed that three strong peaks occurred at 178.66, 551.38, and 737.68 cm⁻¹ points of the α-Fe₂O₃ phase, and two weak peaks occurred at 242.63 and 409.40 cm⁻¹ points (Figure 2). According to XPS measurements of silicon-doped Si:Fe₂O₃ thin films, it was observed that the peaks shifted towards lower values and there was a weakening in the peak intensities. The peaks at 551.38 and 737.68 cm⁻¹ belong to the Fe₃O₄ structure, and no γ-Fe₂O₃ peak was found at 350, 500 and 700 cm⁻¹ (Jubb et al., 2010). It was concluded that the Fe₃O₄ structure may emerge due to the transformation of Fe³⁺ ions into Fe²⁺ during the reaction and the octahedral regions being occupied by Fe²⁺ ions.

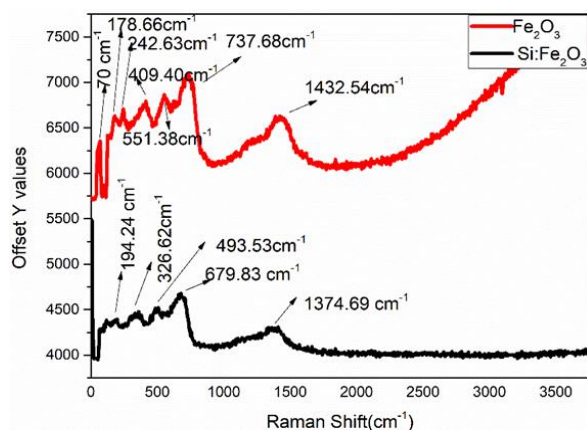


Figure 2. Raman Shift measured at room temperature

XRD diffraction patterns and SEM image showed that the lattice parameters gradually decreased with the increase of silicon doping. In the SEM image (Figures 3(a), 4(a)), it was observed that the structure was distributed quite homogeneously on the substrate. The surface morphology of Si:Fe₂O₃ and Fe₂O₃ structured thin films was analyzed

using the non-contact mode of AFM (Fig. 3(b), 4(b)). Figures 3(b), 4(b) show 2D and 3D AFM images of Si:Fe₂O₃ and Fe₂O₃ structure grown on glass substrates. The roughness values of the film were determined to be Ra=3.08 nm, Sa=2.7 nm (Si:Fe₂O₃) and Ra=1.88 nm, Sa=2.09 nm (Fe₂O₃), respectively.

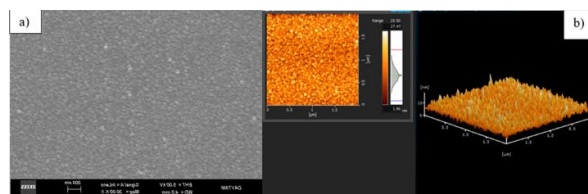


Figure 3. (a) SEM and (b) 2D-3D AFM images of the Si:Fe₂O₃ thin film

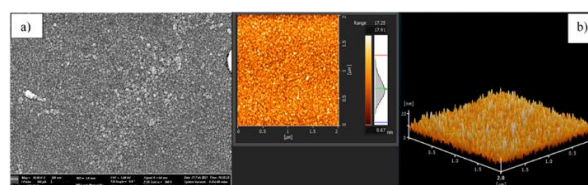


Figure 4. (a) SEM and (b) 2D-3D AFM images of the Fe₂O₃ thin film

X-ray photoelectron spectroscopy (XPS) is a very useful and effective technique used to determine the chemical bonds on the surfaces of materials and within the structure. This technique is generally based on the calibration of the chemical binding energy (BE) scale of the particles in the structure. This analysis is a technique based on comparing the spectrum of the carbon layer exposed to air on its surface, using the C1s spectrum of the material as a reference. This technique is the relatively common method used today for all sample types. The source voltage of the x-ray source used for measurements in the study was kept constant at 15 kV and its power at 400 W. The unloaded C1s signal of the calibrated device was kept between 284.5 eV and 285 eV. In the measurements, the spectra of all metallic samples cleaned by spraying argon (Ar) were evaluated according to Au 4f7/2 at an energy of 83.95 eV. As can be seen from the XPS Figures (5 (a), (b), (c), (d)); Although the binding energy of the iron element is normally 706.7 eV, this value was calculated as 709.13-711.77 eV on average in the iron oxide structure and 714.50 eV in the iron-silicon oxide structure. While the binding energy of the silicon element is 90.2 eV,

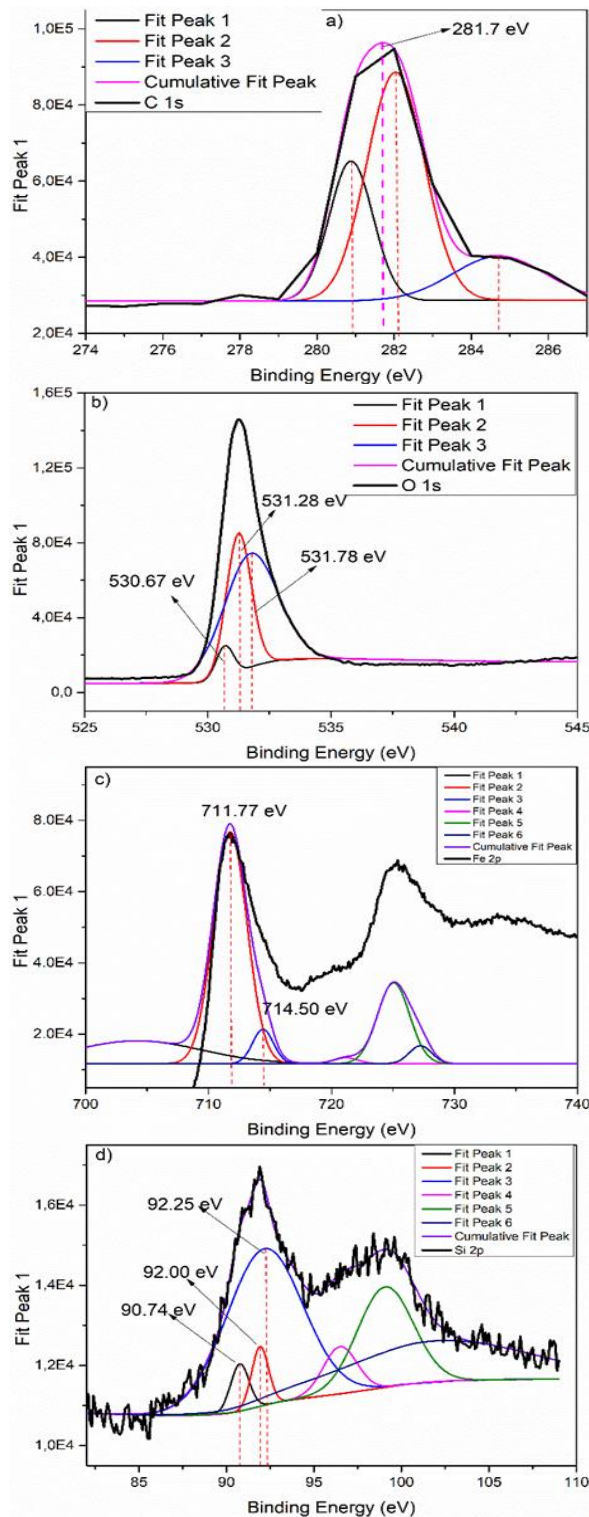


Figure 5. (a) XPS spectra for multi peak fit for C1s (b) O1s and (c) Fe 3p (d) Si 2p of Si:Fe₂O₃ thin film

this value increased to 90.74-92.25 eV on average in the iron oxide structure.

This change in binding energy is due to the electron exchange of silicon-iron with oxygen, and in the iron - silicon oxide structure, this energy increases slightly with the chemical

environment effect.

One of the most used methods for determining the band edges and band gap energy of semiconductor thin films is the absorption measurement method. In our study, absorption measurements of semiconductor thin films grown on glass substrate were obtained at room temperature using a Perkin Elmer UV/Visible Lambda 2S spectrometer with a spectrometric measurement range of 200-1100 nm.

In addition, the direct optical band gaps of the samples were calculated with Tauc's law,

$$(\alpha \times hv) = A (hv - E_g)^2 \quad (2)$$

where α is the absorption coefficient, h is Planck's constant, ν is the photon's frequency, A is a proportionality constant, In the above expression, E_g is the band gap of the semiconductor and the value of n is a parameter that varies depending on whether the band gap energy of the material has a direct or indirect transition (Viezbicke et al., 2015). As a result of the calculations made with Equation (2), the band gaps of the semiconductors were found by drawing the graph in Figure 6(a-b).

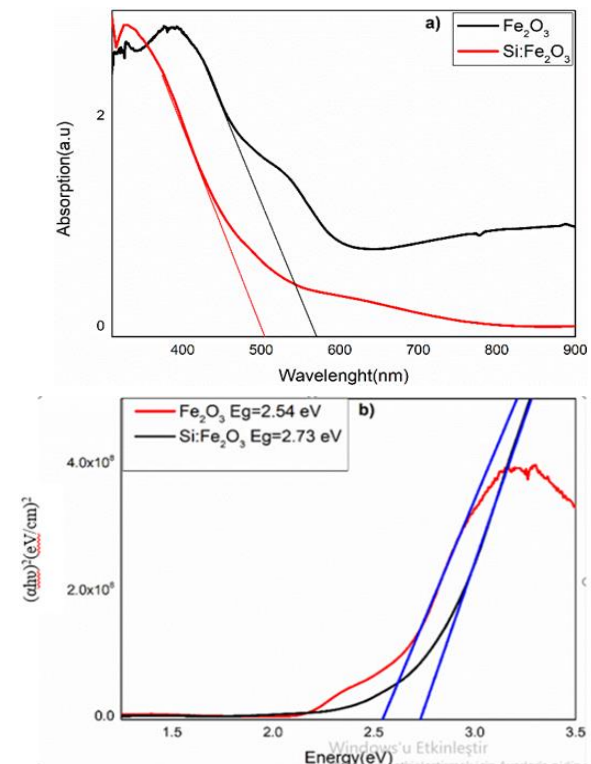


Figure 6. (a) Absorption and (b) band gap graph of Si:Fe₂O₃ and Fe₂O₃ structure

As a result of optical measurements, it was seen that the band gap of the structure was between 2.54-2.73 eV. Figure 6(a) shows the Tauc plot corresponding to the absorption spectra. It was calculated using the Tauc Equation that the band structure of thin films has a direct optical band gap. It was observed that with the doping of Si into the Fe₂O₃ structure, there was an increase of 0.19 eV in the band gap. As seen in Figure 6(a), the absorption amount and absorption wavelength changed as a result of the doping process of the thin film. Thus, it was observed that a widening occurred in the optical band gap of the semiconductor (Figure 6(b)). Since the defects at the edge of the iron oxide band are closed by silicon, the band gap energy has increased and the absorption has decreased.

4. Conclusion

In our study, as seen from the XRD diffraction curve, it was observed that the maghemite iron oxide (Fe₂O₃) semiconductor was in the tetragonal phase and had very high peak values at 18.42°, 33.55°, 56.69°. Likewise, it was observed that the silicon-doped iron oxide (Si:Fe₂O₃) compound was in the tetragonal phase and had a high peak intensity at 30.41°.

The binding energy of the iron element is 706.7 eV, and it has been observed that this value increases to 709.13-711.77 eV on average in the iron oxide structure and is 714.50 eV in the iron-silicon oxide structure. While the binding energy of the silicon element is 90.2 eV, this value increased to 90.74-92.25 eV on average in the iron-oxide structure. This increase in binding energy is due to the electron exchange of silicon-iron with oxygen, and in the iron-silicon oxide structure, this energy increases slightly due to the effect of the chemical environment.

As a result, XRD diffraction measurements for structural characterization showed that crystal grain sizes decreased with increasing silicon ratio in the structure. The Si⁴⁺ cation in spinel-like structures showed a strong distribution tendency in the tetrahedral region, which was affected by the oxygen amount parameter in the structure.

XRD and SEM images show that crystal grain sizes gradually decrease as the silicon ratio in the structure increases. In the SEM image, it was seen that the structure was distributed quite homogeneously on the substrate.

Author contribution

All studies for the article, such as material procurement, data collection, data processing, literature review, writing, and critical review, were carried out by Author Erdal TURGUT.

Acknowledgment: We would like to thank the Atatürk University Eastern Anatolia High Technology Application and Research Center (DAYTAM) for their support.

Funding declaration

This research has not received a specific grant from any commercial or non-commercial funding agency.

Conflict of Interest Statement

The author(s) declare that they have no conflict of interest.

Ethical standards

No Ethics Committee Approval is required for this study.

References

- Bali, M. and Muetze A., (2017). Modeling the effect of cutting on the magnetic properties of electrical steel sheets. *IEEE Transactions on Industrial Electronics*, 64 (3), 2547–2556. <https://doi.org/10.1109/TIE.2016.2589920>
- Bourchas, K., Stening, A., Soulard, J., Broddefalk, A., Lindenmo, M., Dahlen, M., Gyllensten, F. (2016). Influence of cutting and welding on magnetic properties of electrical steels. *2016 XXII International Conference on Electrical Machines (ICEM)*, 04-07 September 2016, Lausanne, Switzerland. <https://doi.org/10.1109/ICELMACH.2016.7732770>

- Chu, M., Shao, Y., Peng, J., Dai, X., Li, H., Wu, Q. and Shi, D. (2013). Near-infrared laser light mediated cancer therapy by photothermal effect of Fe₃O₄ magnetic nanoparticles. *Biomaterials*, 34(16), 4078-4088. <https://doi.org/10.1016/j.biomaterials.2013.01.086>
- Chomoucka, J., Drbohlavova, J., Huska, D., Adam, V., Kizek, R. and Hubalek, J. (2010). Magnetic nanoparticles and targeted drug delivering. *Pharmacological Research*, 62(2), 144-149. <https://doi.org/10.1016/j.phrs.2010.01.014>
- Gasparov, L.V., Tanner, D.B., Romero, D.B., Berger, H., Margaritondo, G., Forro L. (2000). Infrared and Raman studies of the Verwey transition in magnetite. *Physical Review B*, 62(12), 7939–7944. <https://doi.org/10.1103/PhysRevB.62.7939>
- Helbling, H., Benabou, A., Van Gorp, A., El Youssef, M., Tounzi, A., Boughanmi, W., Laloy, D. (2020). Effect on magnetic properties of inhomogeneous compressive stress in thickness direction of an electrical steel stack. *Journal of Magnetism and Magnetic Materials*, 500, 166353. <https://doi.org/10.1016/j.jmmm.2019.166353>
- Hu, F., Macrenaris, K.W., Waters, E.A., Schultz-Sikma, E.A., Eckermann, A.L., Meade, T.J. (2010). Highly dispersible, superparamagnetic magnetite nanoflowers for magnetic resonance imaging. *Chemical Communications*, 46(1), 73-75. <https://doi.org/10.1039/b916562b>
- Jubb, A.M. and Allen, H.C. (2010). Vibrational spectroscopic characterization of hematite, maghemite, and magnetite thin films produced by vapor deposition. *Applied Materials and Interface*, 2(10), 2804–2812. <https://doi.org/10.1021/am1004943>
- Leary, A.M., Ohodnicki, P.R., McHenry, M.E. (2012). Soft magnetic materials in highfrequency, high-power conversion applications. *JOM*, 64 (7), 772–781. <https://doi.org/10.1007/s11837-012-0350-0>
- Lee, C.Y., Wang, L., Kado, Y., Kirchgeorg, R., Schmuki, P. (2013). Si-doped Fe₂O₃ nanotubular/nanoporous layers for enhanced photoelectrochemical water splitting. *Electrochemistry communications*, 34, 308-311. <https://doi.org/10.1016/j.elecom.2013.07.024>
- Piekarz, P., Oleś, A.M., Parlinski, K. (2010). Comparative study of the electronic structures of Fe₃O₄ and Fe₂SiO₄. *arXiv*, 1007.2340. <https://doi.org/10.48550/arXiv.1007.2340>
- Qayoom, M., Shah, K.A., Pandit, A.H. (2020). Dielectric and electrical studies on iron oxide (α -Fe₂O₃) nanoparticles synthesized by modified solution combustion reaction for microwave applications. *Journal of Electroceramics*, 45, 7–14. <https://doi.org/10.1007/s10832-020-00219-2>
- Schoppa, A., Schneider, J., Wuppermann, C-D., Bakon, T. (2003). Influence of welding and sticking of laminations on the magnetic properties of non-oriented electrical steels. *Journal of Magnetism and Magnetic Materials*, 254-255, 367–369. [https://doi.org/10.1016/S0304-8853\(02\)00877-6](https://doi.org/10.1016/S0304-8853(02)00877-6)
- Shokrollahi, H. and Janghorban K., (2007). Soft magnetic composite materials (SMCs). *Journal of Materials Processing Technology*, 189 (1-3), 1–12. <https://doi.org/10.1016/j.jmatprotec.2007.02.034>
- Silveyra, J.M., Ferrara, E., Huber, D.L., Monson, T.C. (2018). Soft magnetic materials for a sustainable and electrified world. *Science*, 362 (6413), eaao0195. <https://doi.org/10.1126/science.aao0195>
- Uebe, R., Henn, V. and Schüler, D. (2012). The mag protein of magnetospirilla is not involved in bacterial magnetite biomineralization. *Journal of Bacteriology*, 194(5), 1018-1023. <https://doi.org/10.1128/JB.06356-11>
- Viezbicke, B.D., Patel, S., Davis, B.E., Birnie, D.P., III. (2015). Evaluation of the Tauc method for optical absorption edge determination: ZnO thin films as a model system. *Physica Status Solidi (b)*, 252(8), 1700-1710. <https://doi.org/10.1002/pssb.201552007>
- Wei, X., Liu, T., Li, J., Chen, X. (2011). A magnetic-controlled amperometric biosensor based on composite bio-particulates Fe₃O₄ and nano-au with the signal enhancement by increasing loading of horseradish peroxidase. *International Journal of Electrochemical Science*, 6(10), 4953-4966. [https://doi.org/10.1016/S1452-3981\(23\)18380-5](https://doi.org/10.1016/S1452-3981(23)18380-5)
- Xiao, L., Li, J., Brougham, D.F., Fox, E.K., Feliu, N., Bushmelev, A., Schmidt, A., Mertens, N., Kiessling, F., Valldor, M., Fadeel, B., Mathur S.

- (2011). Water-soluble superparamagnetic magnetite nanoparticles with biocompatible coating for enhanced magnetic resonance imaging. *ACS Nano*, 5(8), 6315-6324. <https://doi.org/10.1021/nn201348s>
- Xiong, C.J., Yuan, X.H., Zhou, J.D., Chen, Y., Chen, F.H., Xu, L.X. (2013). Synthesis of folic acid-modified Fe₃O₄ nano-magnetic fluid for in vivo tumor cell labeling. *African Journal of Pharmacy and Pharmacology*, 7(12), 666-672.
- Yamazaki, K. And Fukushima, W. (2015). Loss analysis of induction motors by considering shrink fitting of stator housings. *IEEE Transactions on Magnetics*, 51 (3), 1-4. <https://doi.org/10.1109/TMAG.2014.2357842>
- Zhang, Z., Wang, X. and Yang, X. (2011). A sensitive choline biosensor using Fe₃O₄ magnetic nanoparticles as peroxidase mimics. *Analyst*, 136(23), 4960-4965. <https://doi.org/10.1039/C1AN15602K>
- Zhu, S., Guo, J., Dong, J., Cui, Z., Lu, T., Zhu, C., Zhang, D., Ma, J. (2013). Sonochemical fabrication of Fe₃O₄ nanoparticles on reduced graphene oxide for biosensors. *Ultrasonics Sonochemistry*, 20 (3), 872-880. <https://doi.org/10.1016/j.ultsonch.2012.12.001>